The finite-state character of physical dynamics

Norman Margolus

Massachusetts Institute of Technology, Cambridge MA 02139. `nhm@mit.edu`

Finite physical systems have only a finite amount of distinct state. This finiteness is fundamental in statistical mechanics, where the maximum number of distinct states compatible with macroscopic constraints defines *entropy*. Here we show that finiteness of distinct state is similarly fundamental in ordinary mechanics: *energy* and *momentum* are defined by the maximum number of distinct states possible in a given time or distance. More generally, *any moment of energy or momentum* bounds distinct states in time or space. These results generalize both the Nyquist bandwidth-bound on distinct values in classical signals, and quantum uncertainty bounds. The new *certainty bounds* are achieved by finite-bandwidth evolutions in which time and space are effectively discrete, including quantum evolutions that are effectively classical. Since energy and momentum count distinct states, they are defined in finite-state dynamics, and they relate classical mechanics to finite-state evolution.

INTRODUCTION

We live in a world that, like a digital photograph, has only finite resolution. This was first recognized in statistical mechanics, when Planck introduced a finite grain-size h to get a realistic counting of distinct states [1, 2]. Once it was understood that h relates all energy and momentum to waves [3, 4], finite resolution was explained as a property of waves: a tradeoff between range of frequencies superposed and maximum localization [5–19].

There is also a tradeoff, in superpositions of waves, between frequency range and *average* localization. This is known in communications theory as the Nyquist bound: a finite bandwidth signal can carry only a finite number of distinct values per unit length. This holds because a finite number of Fourier components can add up to chosen values at only a finite number of places [20].

In this paper, we combine and generalize these tradeoffs. We count *how many* quantum states can be distinguished from each other *with certainty*, in a finite time or distance, given average constraints on wavefunction bandwidth. These *certainty bounds* redefine energy and momentum as maximum counts, and challenge the distinction between continuous and discrete in physics.

To illustrate the connection between bandwidth and distinct quantum states, consider a free particle moving in one dimension, in a periodic space of length L. Momentum eigenstates must have a whole number of oscillations in period L, so allowed spatial frequencies p_n/h are $1/L$ apart. A wavefunction using N different spatial frequencies must have at least $N-1$ times this minimal separation, between minimum and maximum frequencies:

$$\frac{p_{\max} - p_{\min}}{h} \geq \frac{N-1}{L} . \tag{1}$$

This is a bandwidth bound for a superposition of N distinct energy-momentum eigenstates. It also bounds the total number of distinct states that can occur as the particle moves a distance L: N distinct eigenstates can add up to at most N distinct sums. Similar arguments apply to energy and time, for an evolution periodic in time [26].

More generally, *any absolute moment* of energy or momentum is an average measure of the frequency-width of

the wavefunction, and can play the role that momentum-bandwidth does in (1), determining a maximum count of distinct states for *any portion of any evolution* with that moment. For $N = 2$ these tradeoffs become minimum uncertainty relations. To achieve the maximum count, the wavefunction must use a finite range of frequencies. Then the exact evolution can be interpolated from the state on a discrete set of points in space and time [21–35].

Perhaps the most interesting moment is average energy above the minimum possible [13]. What we call *energy* classically, counts how many distinct states can occur in a unit of time. How much change. How many distinct computational steps. We can also count just the distinct states due to overall motion, by comparing energy counts in rest and non-rest frames. Surprisingly, motional change is bounded not by the kinetic energy $E - mc^2$, but by pv instead. This difference makes the classical action a count of possible distinct states. It also defines an ideal momentum in finite-state dynamics [27]. Of course, energy also bounds what can be distinguished experimentally. For example, using optics [36–40], with n photons of the same frequency there are at most $2n + 1$ distinct phases within one cycle of oscillation, according to (2).

Below, we first establish energy bounds on the maximum number of states distinguishable-with-certainty that can occur in a given time. We then establish related certainty bounds on overall motion, and discuss finite distinctness in classical dynamics. The arguments used are elementary, and the results are verified numerically.

DISTINGUISHABILITY IN TIME

For an evolution with period T, passing through N distinct (mutually orthogonal) states at a *constant rate* [13],

$$\frac{2(E - E_0)}{h} \geq \frac{N-1}{T} , \tag{2}$$

where E_0 is the lowest energy eigenvalue used in constructing the system's state. The left side is, as in (1), a measure of the width of an eigenfrequency distribution: twice the average half-width. The right side is, again, the minimum

frequency width for N distinct states. We show that (2) holds even if the time intervals between distinct states are unconstrained. Then, letting τ be the average time separating consecutive distinct states, (2) becomes

$$(E - E_0)\,\tau \geq \frac{N-1}{N}\frac{h}{2}\;. \qquad (3)$$

We show (3) also holds for a *portion of an evolution*, comprising N distinct states with average separation τ. For $N = 2$ this becomes the minimum separation bound [13]. We provide similar bounds for other moments of energy.

We formalize our problem as a minimization. Consider a finite-sized isolated system with a time evolution expressed as a superposition of energy eigenstates:

$$|\psi(t)\rangle = \sum_n a_n e^{-2\pi i \nu_n t}|E_n\rangle\;, \qquad (4)$$

with $\nu_n = E_n/h$. We define a set of average frequency widths (moments) about a frequency α:

$$\langle \nu - \alpha \rangle_M \equiv \left(\sum_n |a_n|^2\,|\nu_n - \alpha|^M\right)^{\frac{1}{M}}\;, \qquad (5)$$

with $M > 0$ (other measures of overall width could also be used, *e.g.* [9]). If evolution (4) passes through a series of mutually orthogonal states $|\psi(t_k)\rangle$ at times t_k, then

$$\langle \psi(t_m)|\psi(t_k)\rangle = \sum_n |a_n|^2 e^{2\pi i \nu_n(t_m - t_k)} = \delta_{mk}\;. \qquad (6)$$

We seek the minimum frequency widths (5) of states satisfying the constraints (6) for any sequence of N distinct states within a time interval of length T_N.

We assume, *without loss of generality*, that all ν_n are distinct (in both (5) and (6), coefficients for a repeated ν_n can be consolidated), and that overall evolution is periodic with some recurrence-time [41] T that may be much longer than T_N. Then the discrete spectrum, bounded from below [42], includes *at most* all of the frequencies

$$\nu_n = \nu_0 + n/T\;, \qquad (7)$$

with n a non-negative integer. These are all of the possible eigenfrequencies of energy eigenstates that cycle with period T, up to an overall phase. This spectrum restricts the *maximum period* to be T, but evolution can repeat more than once in this time. For T sufficiently large (7) approaches a continuous spectrum, allowing us to minimize over the union of all possible discrete spectra.

We first consider an evolution with a constant rate of distinct change. If $N > 1$ distinct states have equal separations τ within period $T = N\tau$, then $t_m = m\tau$ and from (6) and (7),

$$\langle \psi(t_{k+m})|\psi(t_k)\rangle = e^{2\pi i \nu_0 t_m}\sum_{n=0}^{\infty}|a_n|^2 e^{2\pi i n m/N}\;. \qquad (8)$$

There are only N distinct phases in the sum (8), so we can minimize all $\langle \nu - \alpha \rangle_M$ for a given α by using a set of
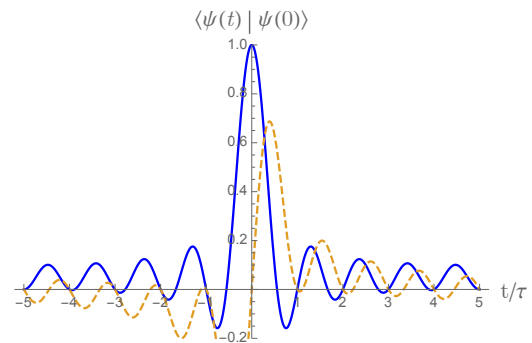

FIG. 1. *A periodic evolution with N distinct states τ apart* (solid real, dashed imaginary, depicted for $N = 10$). Only a discrete set of frequencies fit the period: all are allowed in the minimization. An equally weighted superposition $|\psi(t)\rangle$ of N consecutive frequencies is the narrowest that gives N distinct states in time. Centered on α, it minimizes all $\tau\,\langle \nu - \alpha \rangle_M$.

N consecutive ν_n's, centered as closely as possible on α: we get the same orthogonality times in (8) with smaller width (5) by setting each $|a_n|^2$ outside the set to 0, and transferring its weight to the equivalent phase within the set. Then, since $\langle \psi(t_{k+m})|\psi(t_k)\rangle = \delta_{m0}$, the N consecutive non-zero $|a_n|^2$ are just the discrete Fourier transform of a Kronecker delta impulse, and so they all equal $1/N$. Thus all $\langle \nu - \alpha \rangle_M$ are minimized by an equal superposition with minimum bandwidth for N distinct states (illustrated in Figure 1), so the dimensionless product

$$\tau\,\langle \nu - \alpha \rangle_M \;\geq\; f_\alpha(M, N) \qquad (9)$$

for some $f_\alpha(M, N)$ defined by the minimizing state. For example, if $\alpha = \nu_0$, the closest to centering a minimum bandwidth state on α is for ν_0 to be the lowest frequency. Then equality in (9) requires N equal $|a_n|^2$ in (5), and

$$f_{\nu_0}(M, N) = N^{-(1+\frac{1}{M})}\left(\sum_{n=0}^{N-1} n^M\right)^{\frac{1}{M}}\;. \qquad (10)$$

For $M \geq 1$ this ranges from $1/4$ to 1. $f_{\nu_0}(1, N)$ gives (3).

Similarly, if α is the midpoint of N consecutive frequencies ν_n, a minimum bandwidth state can be exactly centered on the mean frequency $\bar{\nu} = \alpha$, and

$$f_{\bar{\nu}}(M, N) = N^{-(1+\frac{1}{M})}\left(\sum_{n=0}^{N-1}\left|n - \frac{N-1}{2}\right|^M\right)^{\frac{1}{M}}\;. \qquad (11)$$

For $M \geq 1$ this ranges from $2/9$ to $1/2$, and is the smallest achievable bound: no other α gives a smaller bound. For $0 < M < 1$, however, $\alpha = \nu_n$ (an eigenfrequency) is better for even N (even though a minimum bandwidth state can't be exactly centered on α in this case). Excluding $f_{\bar{\nu}}$ for $M < 2$, both f_{ν_0} and $f_{\bar{\nu}}$ strictly increase with N.

Now consider an evolution with a constant rate portion. Suppose there are N distinct states, spaced τ apart, within an interval T_N. To find the minimum of $\tau\,\langle \nu - \alpha \rangle_M$ we assume evolution outside of T_N puts no constraints on the minimization problem: it adds no orthogonality constraints, and the maximum period T is unbounded so all frequencies are allowed in (7).
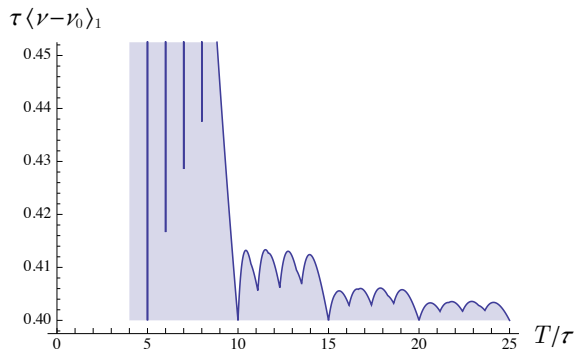
FIG. 2. *Minimum of $\tau\langle\nu-\nu_0\rangle_1$ for an evolution with maximum period T that includes $N = 5$ distinct states, τ apart. Each choice of T constrains the frequency spectrum, and the corresponding minimum is determined numerically. The minimum for $T = N\tau$ (bottom of shaded area) recurs, and is the minimum for $T \to \infty$, the case of an unconstrained spectrum.*

FIG. 3. *For each of 12,000 sets of separations between distinct states, we compare the minimum of E with the minimum E_{bound} possible if all separations were equal. Each evolution is periodic with period T, and we group them based on the number $N_{\mathrm{different}}$ of different separation lengths between consecutive distinct states. $E > E_{\mathrm{bound}}$ unless $N_{\mathrm{different}} = 1$.*

We find, in general, that the optimal evolution containing T_N repeats with period $N\tau$, and so the bounds are again $f_\alpha(M, N)$. We see this in the example of Figure 2, plotting the minimum of $\tau\langle\nu - \nu_0\rangle_1$ with $N = 5$ for different T (for numerical methods see Appendix A). The global minimum recurs whenever T is an integer multiple of $N\tau$, so the bound for $T = N\tau$ holds for $T \to \infty$.

The general behavior is clear for large M: the minimum bandwidth state is the minimizing state, since $\tau\langle\nu - \alpha\rangle_\infty$ *is* the (dimensionless) bandwidth. Minimum bandwidth requires repetition with period $N\tau$, since otherwise there are too many constraints (6) to satisfy. Similarly for large N, the constant-rate bounds $f_\alpha(M, N)$ apply as long as $f_\alpha(M, N)$ increases monotonically with N, since the limit $N \to \infty$ is also the limit $T = N\tau \to \infty$.

The situation is much the same for small M and N. If we take the limit $T \to \infty$ with T an integer multiple of τ then, since $t_m = m\tau$, for each T there are only T/τ distinct phases in (6), and so only a finite bandwidth $1/\tau$ is relevant to the minimization in the limit. We surveyed ten thousand cases numerically (some illustrated in Figures 5–8 of Appendix A) and found that the minimizing bandwidth is slightly smaller: $(N - 1)/N\tau$, the minimum possible (which requires repetition with period $N\tau$). The only exceptions were some moments about $\bar{\nu}$ with $M < 2$ and N even, where the minimizing bandwidth was $1/\tau$. For these moments, the increase of $f_{\bar{\nu}}(M, N)$ with N is non-monatonic: it decreases going from even to odd. Thus allowing one more distinct state (or one more frequency) when N is even decreases the bound.

Equal separation is not an assumption for $N = 2$, since there is only one separation. Known bounds on orthogonality time agree with with $f_\alpha(M, 2)$ [7, 8, 13, 15, 16].

Finally, if equal separation is optimal, constant rate bounds hold with τ the *average separation*. Intuitively, inequality requires some separations to be smaller than average, and it is the smallest separations in an evolution that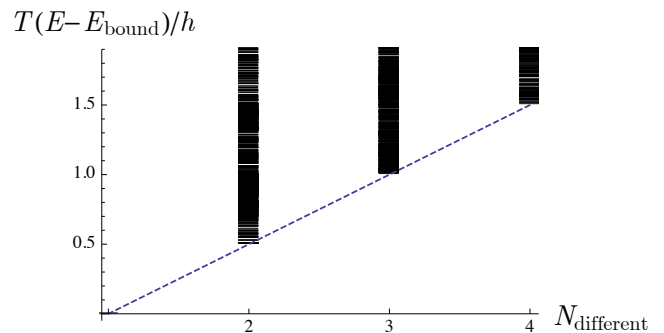 require the largest frequency widths, hence equality is optimal. More formally, consider an evolution with N distinct states in period T. There are N different intervals $T_N < T$ that encompass all N of the distinct states, each omitting one separation from T. Since there is a positive minimum value for the dimensionless product $T_N \langle\nu - \alpha\rangle_M$, the smallest T_N requires the largest $\langle\nu - \alpha\rangle_M$. Thus the best we can do is make all T_N equal, and hence all separations equal.

Alternatively, we can observe that the number of constraints (6) on the minimization problem grows rapidly as the number $N_{\mathrm{different}}$ of different-length separations required in the evolution increases, and these additional constraints increase the minimum even when the lengths are almost exactly equal. This is illustrated in Figure 3, which compares the minimum average energy E, determined numerically for 12,000 random sets of separations in periodic evolutions, to the equal-separations minimum $E_{\mathrm{bound}} = h(N - 1)/2T + E_0$ given by (2). E_{bound} is only achievable if $N_{\mathrm{different}} = 1$. The dashed line is approached by almost-equal separations. As long as the separations aren't exactly equal the minimum is altered by a discrete jump for each additional length: requiring $\langle\psi(t)|\psi(0)\rangle = 0$ for times arbitrarily close to equal separation essentially adds a slope $= 0$ constraint at equal separations (which results in the dashed line), so average energy is greater. Other cases are similar (see Figures 9–12 in Appendix A).

The moment bounds are achievable: exactly for spectra that include N evenly spaced energy eigenvalues, and approximately for almost even spacing. In the macroscopic limit, they are achieved by states that have a uniform probability density for a range of energies [13], which is nearly the case for very complicated evolutions (see Appendix B). Moreover, energy can always be moved to a system where (3) is achievable, so *average energy is equivalent to a count of possible distinct states per unit time.*

States that achieve a moment bound have essentially minimal bandwidth, making continuous evolution an interpolation of a discrete one with the widest possible spacing between discrete states (see Appendices D and E).
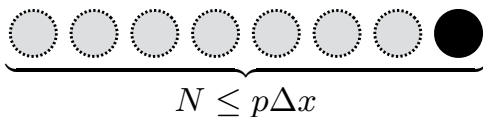
$$N \leq p\Delta x$$

FIG. 4. *We see extra distinct states of a particle when there is relative motion, and we see it as having more than its rest energy.* We can count the extra states based on the extra energy. For $N \gg 1$ and using units with $h = 2$, maximum distinct states in the lab frame is $E\Delta t$, in the rest frame $E_r\Delta t_r$, and so the difference $p\Delta x$ is due to overall motion.

DISTINGUISHABILITY IN SPACE

For an isolated system in motion, some distinct states can be attributed to the motion. We can determine how many by comparing with the same evolution seen in its rest frame: any extra distinct states when moving must be due to the motion. Energy bounds the number of distinct states in each frame, yielding a bound on motion (*cf.* [3]):

$$p\lambda \geq \frac{N-1}{N}\frac{h}{2} . \qquad (12)$$

Here p is the magnitude of the system's average momentum, and λ is the average separation in space within a sequence of N states that are distinct due to the motion. Similar bounds hold for other moments of momentum.

We first count macroscopically, in two frames. Assuming $N \gg 1$, set $h = 2$ and take the energy of flat empty space to be $E_0 = 0$ in both frames [42, 43]. Then (3) becomes $1/\tau \leq E$, and energy is the maximum average rate of distinct state change physically possible.

In the laboratory frame, in a time interval Δt, an isolated system evolves through at most $E\Delta t$ distinct states. Meanwhile, moving at speed v, it travels a distance $\Delta x = v\Delta t$. In the corresponding rest frame evolution, at most $E_r\Delta t_r$ states are distinct. The difference, which is a familiar relativistic quantity

$$E\Delta t - E_r\Delta t_r = p\Delta x , \qquad (13)$$

counts the extra distinct states possible in the frame where there is overall motion (Figure 4). Thus p is the extra per unit distance, agreeing with (12) for $N \gg 1$.

Dividing (13) by Δt, we see that $E - E_r/\gamma = vp$ bounds the average rate of motional state change, even at low velocities. This is slightly surprising, since conventionally the smaller quantity $E - E_r$ is taken as the energy of motion. Indeed, if we model the motion of a free particle by treating its rest energy E_r as its minimum possible energy E_0, then (3) gives $E - E_r$ as the maximum average rate of motional state change, for $N \gg 1$. In general, though, E_r is the average energy of a rest frame dynamics, so $E - E_r$ is the difference of maximum rates in two different frames—which is not a rate in either.

To find precise momentum bounds, consider a constant-speed shift dynamics. With the hamiltonian $\mathsf{H} = v\mathsf{p}_x$, the wavefunction shifts in the $+x$ direction at speed v. If τ is the average time between distinct states, $\lambda = v\tau$ is the average shift between them. Since $E_n = vp_n$, we can let $E_n\tau \to p_n\lambda$ in (9), with $\mu_n = p_n/h$ the spatial frequencies along the direction of motion, giving

$$\lambda\langle\mu - \alpha\rangle_M \geq f_\alpha(M, N) . \qquad (14)$$

This is the general shift-in-space counterpart of the shift-in-time bound (9). If there is no constraint on the lowest frequency in the spatial superposition, then the $\alpha = \bar{\mu}$ bounds apply—the minimizing state is centered on α.

What we seek, however, is more specific: the average separation between states *distinct due to overall motion*. To find this we need a wavefunction that represents only overall motion, and nothing of internal (rest-frame) dynamics. Thus for a massless particle, we must require that all momenta along the direction of motion be positive. Otherwise there will be cancellation of momenta in the superposition, and part of the energy of the wavepacket will actually be rest energy, rather than energy of overall motion. With this restriction the dynamics is a pure shift so the bounds (14) apply, including the $\alpha = \mu_{\min}$ bounds.

The same conclusions hold for a massive particle. The moving wavepacket now has a rest frame, so the only way to avoid seeing *rest-frame changes* in the overall motion is for there to *be none:* a pure shift dynamics. Thus in all cases, overall motion is represented by $\mathsf{H} = v\mathsf{p}_x$ with a positive momentum spectrum, and so $\langle\mathsf{H}\rangle = vp$.

The bounds (14) are consistent with (1), (12), Luo's bound [44] on $\langle|\mathsf{p}|\rangle$, and Yu's bound [12] $\Delta p\,\lambda_{\min} \geq h/4$. In applying bounds (9) and (14) to computation, note that intermediate results may not be distinct [45].

FINITE CLASSICAL DISTINCTNESS

Although bounds on certainty seem quintessentially quantum mechanical, finite distinctness of finite energy dynamics is evident even in the classical realm.

Macroscopic distinctness is governed by macroscopic energy and momentum. Unlike typical small systems [46], macroscopic systems traverse a succession of almost perfectly distinct states as they explore their enormous state spaces: two randomly-chosen d-dimensional normalized states have expected overlap of $1/\sqrt{d}$, so a sequence of states far enough apart in time to each be distinct from the next, should all be nearly distinct.

We can investigate how quickly a complicated dynamics reaches distinct states by studying random dynamics. For random hamiltonian matrices (Appendix B), in the limit where the dimension goes to infinity, with a generic $\psi(0)$ and taking $h = 2$ and $E_0 = 0$, the overlap $\langle\psi(t)|\psi(0)\rangle$ is $2J_1(\pi Et)/\pi Et$. The first zero occurs at $t \approx 1.22/E$, close to the bound $\tau \geq 1/E$. Since the exact dynamics of all the energy in even a tiny portion of a macroscopic system is so complicated, this may provide at least a rough idea of the local rate of distinct change: nearly maximal.

The discretely-distinct character of macroscopic evolution suggests that finite-state systems should be of fun-

damental interest in modeling the classical realm. Historically, this has been true for modeling finite entropy in statistical mechanics [47], but not for modeling finite energy and momentum in dynamics, where classical finite-state models have generally been regarded as mere computational treatments of the "real" continuum dynamics [48, 49]. An exception has been finite-state lattice models isomorphic to continuum models sampled at integer times (see Appendix C). These are closely related to quantum models with a bounded spectrum (see Appendix E).

Macroscopically, if total relativistic energy counts total rate of distinct change, we can divide this count up into different forms of energy, and into hierarchies of almost-isolated sets of degrees of freedom—described by hamiltonians or lagrangians. Just as the hamiltonian counts distinct states, so does the lagrangian (*cf.* [50]). For example, in a system of particles moving freely between collisions, $p_i v_i$ counts distinct changes per unit time due to motion of particle i, so $-L = H - \sum p_i v_i$ counts changes *not* due to free motion: it counts changes due to interaction.

Classical finite-state models have an ideal energy and momentum. From the viewpoint of quantum computation, classical reversible computation is a special case of what a quantum evolution can do [51]. Classical mechanics doesn't have this status, because it has an *infinite rate* of distinct state change. Only classical *finite-state* dynamics can be recast as *finite-energy* quantum dynamics, with distinct classical configurations identified with distinct quantum states (see Appendix D and E). If we find the least-energetic realization mathematically possible, no physical implementation can do better.

A realistic quantum realization is constrained both by certainty bounds and by relativity. For example, if a particle travels at speed v through a long sequence of distinct position states λ apart, its minimum possible momentum is $p = h/2\lambda$, and the energy required by distinct motion is pv. If $v < c$ though, total energy must be larger, since relativistically $E = pv/(v/c)^2 > pv$. We can use this observation to assign a realistic *extensive* ideal-energy to momentum-conserving lattice models [27].

It might seem surprising that it is, in fact, possible to recast a classical finite-state dynamics with perfect locality and determinism, as a quantum hamiltonian dynamics with *continuous* space and time [26]. In this case, finite-distinctness is encoded in the finiteness of the energy and momentum of the initial state. The desired finite-state evolution constitutes a finite set of distinct sample values, which are continuously interpolated in space and time. Quantum bounds on certainty simply reflect finite distinctness in a continuous description.

Classical signals obey a version of the bounds. A classical signal is like the wavefunction of a scalar particle evolving under a one-dimensional shift dynamics, $\mathsf{H} = v\mathsf{p}_x$. Any finite frequency-moment bounds the number N of distinct states in an interval of the quantum evolution, hence at most N points in the interval can have values specified independently, by superposing the distinct states. This generalizes the Nyquist rate [20] from a bandwidth bound to an any-frequency-moment bound.

CONCLUSIONS

In the standard quantum description of nature, time and space are continuous yet distinctness is finite. This is possible because energy and momentum are wave phenomena: constraints on bandwidth impose finite distinctness, just as they do for continuous classical signals. The width between average frequency and lowest is an important constraint, since classical energy and momentum are average frequencies in quantum mechanics. Finite energy and momentum imply finite distinctness in time and space.

Bounds on distinctness are easy to compute. If a periodic evolution traverses N distinct states, the wavefunction must be a superposition of *at least* N energy eigenstates. Any reasonable measure of energy-frequency width is minimized by *exactly* N, equally weighted, with minimally separated frequencies. We illustrate this for frequency moments. More generally, given that a *portion* of an evolution traverses N distinct states, a *complete* periodic evolution with N distinct states and the same average separation minimizes frequency widths—with a few easily identified exceptions. Bounds on *distinctness due to overall motion* are energy bounds for a shift dynamics with a positive spectrum—equivalent to momentum-width bounds.

The fact that *every absolute moment of energy or momentum* bounds the rate of distinct change in time or space seems not to be know; discussions of *quantum speed limits* are, strangely, based on just two moments. The fundamental role of average energy as a conserved distinctness-resource also seems little appreciated. For example, only average energy above a system's lowest energy state can contribute to distinct change *within the system* (*cf.* [43, 52]). Moreover, forms of energy identify forms of distinctness. For example, in a special-relativistic context, the energy pv counts distinct states allowed by overall motion. This lets us infer a minimum total energy by counting distinct changes in space, enabling the construction of finite-state relativistic models [27].

As long as energy is finite, rate of distinct change remains finite no matter how large a system is or how classical its large-scale evolution. At a mesoscopic scale we might generally expect—considering the full dynamics of all energy—that distinctness in time and space is nearly maximal and the quantumness of the distinct states is irrelevant. This suggests that we may be able to interpret classical mechanics *as if the underlying finitely-distinct evolution were classical*, with classical energy and momentum governing discreteness in time and space (*cf.* [53, 54]). This might, for example, allow informational questions about gravity [55–57], modeled as an entropic force [52, 58–61], to be studied classically (*cf.* [62–64]).

Finally, if we can recast classical mechanics as classical finite-state dynamics, we can regard quantum mechanics as *generalizing* classical mechanics—just as quantum computing generalizes classical computing. From this viewpoint, classical mechanical quantities are simple special cases of quantum ones.

Appendix A: Numerical Tests

A Mathematica notebook, containing code and results for numerical experiments that confirm and extend the energy bound analysis above, and generate the graphs in the figures above and below, is available online [65].

The fundamental minimization problem outlined above requires determination of non-negative coefficients $|a_n|^2$ that minimize (5) while satisfying (6) for a given set of separations in time between distinct states, using the spectrum (7). Both the objective function (5) (raised to the M power) and the constraints (6) are linear combinations of the coefficients, so given a set of separations between distinct states, we can find the global minimum to arbitrary accuracy using linear optimization (linear programming). We take separations to be integers, allowing us to deal with only a finite number of $|a_n|^2$ in our minimization: if both the total period T and the time t are integers, then T is the number of distinct phases possible in the constraints (6). Using more than T consecutive $|a_n|^2$ with a given α would increase the frequency moments (5) without allowing any new constraints. Large integer T allows as much resolution in t/T as desired.

In surveying evolutions similar to Figure 2, with a portion constrained to go through N distinct states with equal separations τ (see Figures 5 through 8), the number of consecutive $|a_n|^2$ needed for large T is only about T/τ, rather than T. This is the asymptotically relevant bandwidth $1/\tau$ (discussed earlier), divided by the spacing $1/T$ between allowed frequencies. Neglecting the smallest possible values of T, which give minimum moments too large to appear on our graphs, we find that in our tests, enough $|a_n|^2$ for the largest T is sufficient for all T. Our choice of τ sets the horizontal resolution of the graphs—these examples use $\tau = 43$. For moments about a mean, the position of the mean frequency relative to the other frequency components makes a difference, so minimization for each choice of total period T involves searching a range of width $1/T$ for the α that minimizes $\langle \nu - \alpha \rangle_M$. For $M \geq 1$, the α found is always the mean $\bar\nu$ of the minimizing state—except for $M = 1$ with $T = N\tau$ and N even, in which case all the α give the same minimum. For $0 < M < 1$ we must add a constraint to each optimization problem, that the mean equals the α being tried. Behavior similar to Figure 2 is seen for $\tau \langle \nu - \alpha \rangle_M$ for almost all M (tested for M up to 1000 and for $M = \infty$) and N (tested up to $N = 30$). The only exceptions are moments about $\bar\nu$ with $M < 2$ and N even: in some of these cases the intervals between the deepest local minima are longer than $N\tau$, and in some cases the pattern of minima is less regular. Of course an estimate of the global minimum can always be obtained by simply minimizing any case with large T. In our tests

(see Figure 8), the difference between local maxima and the global minimum falls as T^{-2} asymptotically for finite M, and as T^{-1} for $M = \infty$. The latter result is implied by a large-T bandwidth bound of $1/\tau + 1/T$: we need to round up the asymptotically relevant bandwidth $1/\tau$ to an integer multiple of $1/T$. The $M = \infty$ graphs in all of these figures are obtained from the bandwidths (or bandwidths above the mean) of states that minimize $\tau \langle \nu - \alpha \rangle_M$ for finite M. For all data shown, the minimizing bandwidths are independent of M for ν_0 and, for $M \geq 30$, for $\bar\nu$.

To verify that equal times between distinct states is optimal, we performed experiments with unequal times. For example, for Figure 3 we generated 12,000 sets of separations stochastically; each set dividing a period T into $N \leq 12$ intervals; each set involving $N_{\text{different}} \leq 4$ different interval lengths separating adjacent distinct states. Separations were integers between 1 and 100, except for five sets of separations near 1000. For each set of separations we used the total T of the integer separations as the number of consecutive $|a_n|^2$ to appear in the minimization. We did a fair sampling for each $N_{\text{different}}$, except that half of the choices of number-of-repetitions of a length favored fewer lengths, and half of the choices of a length favored the longer lengths. This helped fill out the cases with lower minima using a short experiment—our original experiment was completely unbiased and required a much larger number of samples. Similar experiments with other moments also verified equal times as optimal.

Since the dashed boundary in Figure 3 is formed by evolutions with almost-equal separations, we investigated those cases extensively (see Figures 9 through 12). As unequal separations converge towards equal ones, the requirement that arbitrarily-close points of the overlap must be zero contribute additional slope-constraints on top of the equal-separation constraints, as shown in Figure 9. The theoretical curves (dashed lines) in Figure 3 and Figure 10 were obtained by minimizing the equal separations cases, with slope $= 0$ constraints added at the equal separations. The triples of data points plotted for each N in Figure 10 used separations differing by one part in 10, 100, and 1000. For each minimization, we let the number of frequency components equal the total integer period T. The minimizations about the mean for $N_{\text{different}} = 5$ used 600 decimal digits of precision. As is evident in the figure, the improvement in the minimum from using smaller and smaller relative differences diminishes rapidly. There are similarly diminishing returns from using very large numbers of $|a_n|^2$ with almost-equal separations. A minimization of $\langle \nu - \nu_0 \rangle_1 T$ (not included in the figures) for $N = 4$ different separations that differ from one another by only one part in 10^6, using 300,000 consecutive $|a_n|^2$, exceeded the difference $\to 0$ limiting value by only about two parts in 10^5. This was mostly accounted for by three very high frequency components. The only other non-zero coefficients were a_{14} and below. Figures 11 and 12 show an example of a portion of evolution with separations that differ from each other by about one part in 10^3.
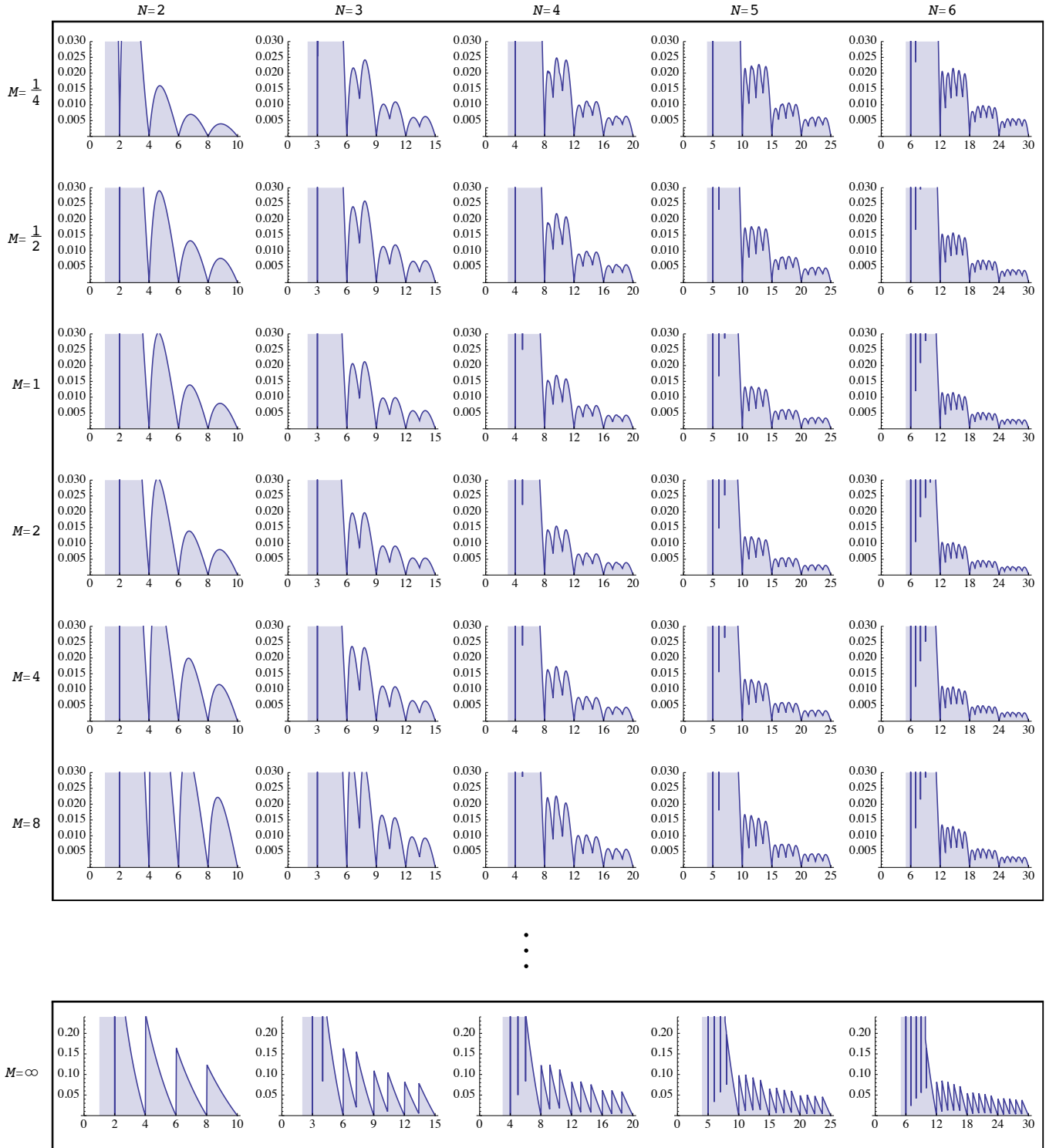
FIG. 5. **Moments about a minimum frequency for a constant rate portion of evolution.** As in Figure 2, the graph at row M and column N shows the minimum value of $\tau \langle \nu - \nu_0 \rangle_M$ for each choice of maximum period T for an evolution that includes N distinct states separated by $N-1$ equal intervals τ, with the horizontal axes labeled with T/τ. For easier comparison, the $T = N\tau$ bound $f_{\nu_0}(M, N)$ is subtracted from each value plotted.
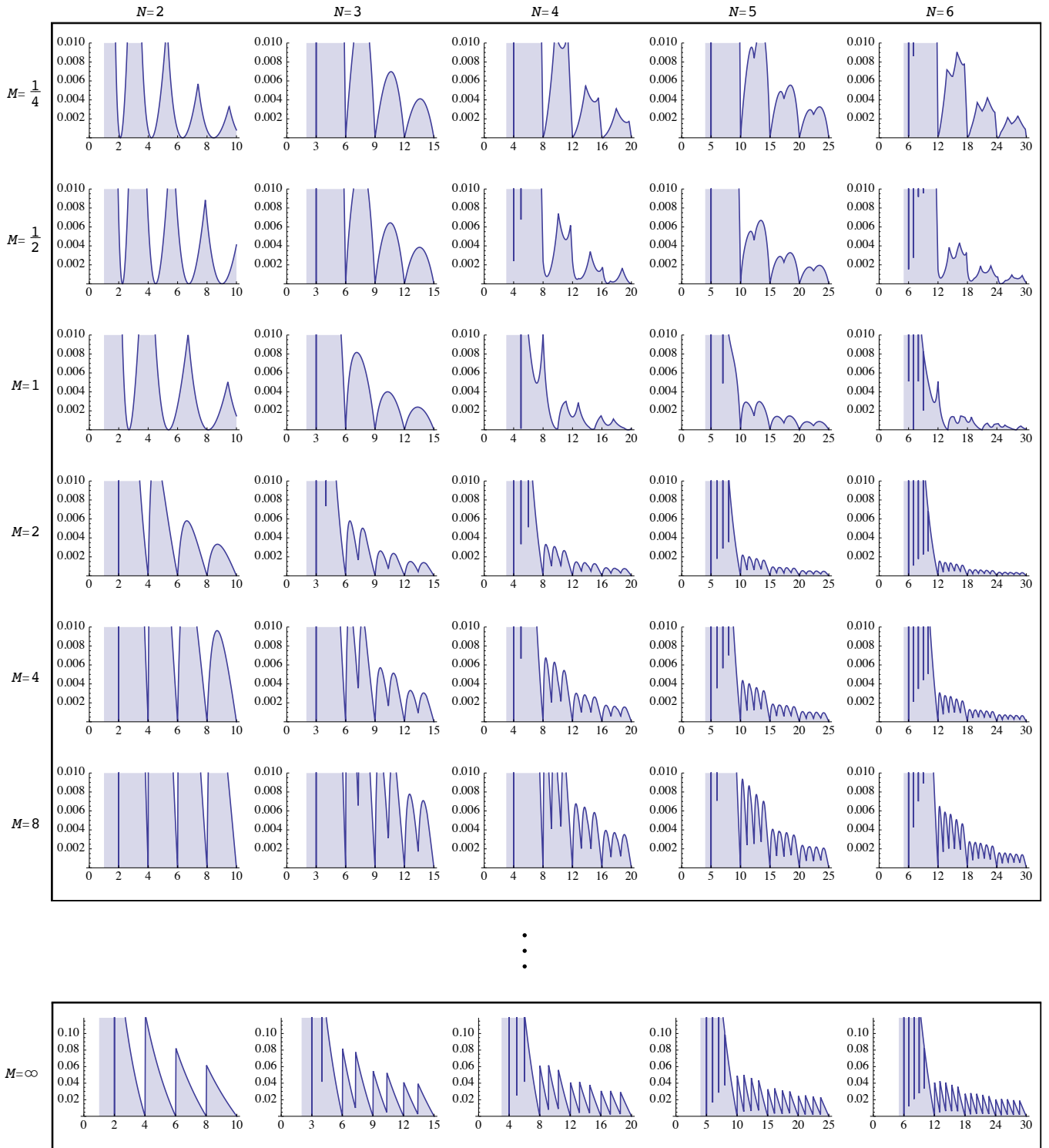
FIG. 6. **Moments about the mean frequency for a constant rate portion of evolution.** The graph at row M and column N shows the minimum values of $\tau \langle \nu - \bar{\nu} \rangle_M$ for each choice of maximum period T for an evolution that includes N distinct states separated by $N - 1$ equal intervals τ, with horizontal axes labeled with T/τ. In each graph the global minimum is subtracted, which is equal to the $T = N\tau$ bound $f_{\bar{\nu}}(M, N)$ except for some $M < 2$ with N even. The case $M = 1$ and $N = 2$ is shown in detail in Figure 13.
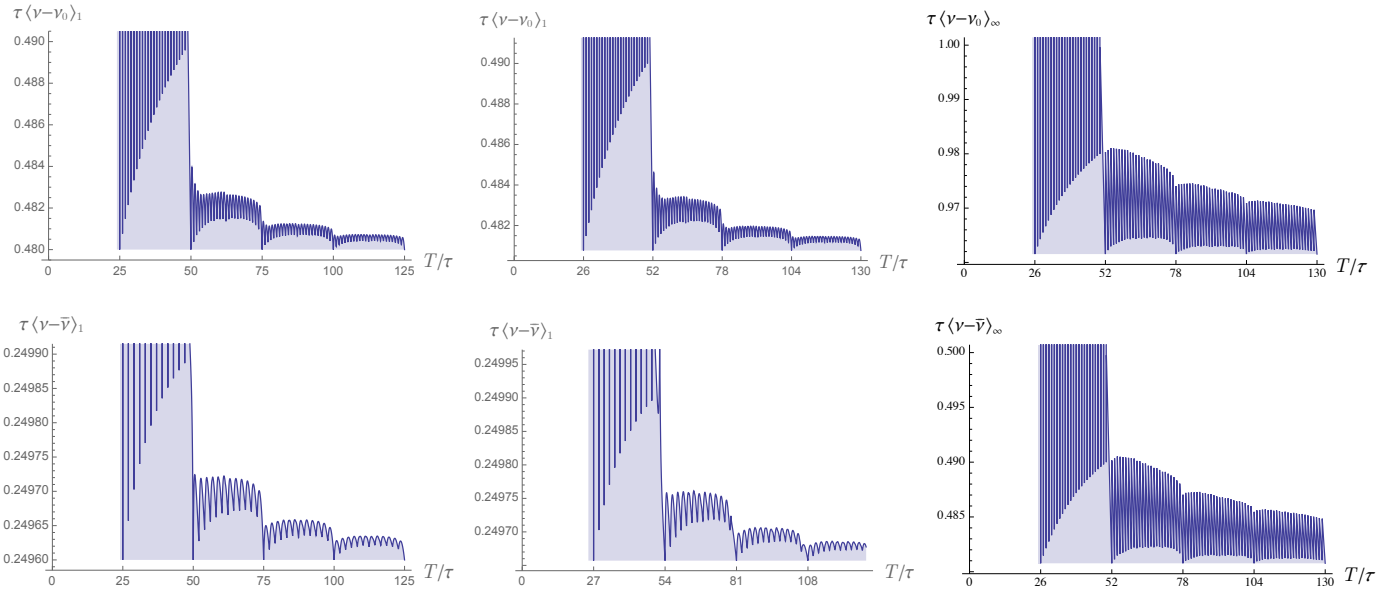
FIG. 7. **Minimizing moments for constant rate portion of evolution, using larger N.** Minimum values are computed numerically for $\tau \langle \nu - \nu_0 \rangle_M$ (first row) and $\tau \langle \nu - \bar{\nu} \rangle_M$ (second row) as we vary the maximum period T, for an evolution that includes N distinct states separated by $N-1$ equal intervals τ. The first column has $N = 25$, the others $N = 26$. All global minima agree with the $T = N\tau$ bound $f_\alpha(M, N)$ except for the bottom middle case, as expected: here the smallest $\tau \langle \nu - \bar{\nu} \rangle_1$ agrees with $.249657 = f_{\bar{\nu}}(1, 27)$, rather than $.25 = f_{\bar{\nu}}(1, 26)$.
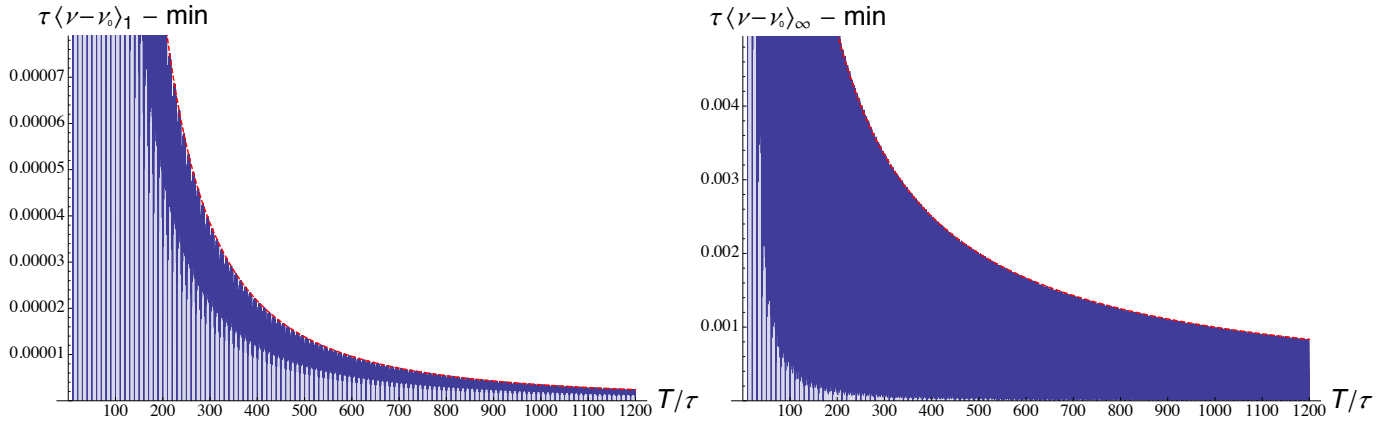

FIG. 8. **Asymptotic behavior of minima with constant rate portion of evolution.** On the left we plot $\tau \langle \nu - \nu_0 \rangle_1$ minus its global minimum, for periodic evolutions of various lengths T that include $N = 10$ distinct states separated by τ; similarly on the right for $\tau \langle \nu - \nu_0 \rangle_\infty$ with $N = 10$. On the left, the red dashed boundary is the function $3.456(T/\tau)^{-2}$. Other finite moments also fall asymptotically like T^{-2}. On the right, the boundary is simply $(T/\tau)^{-1}$. This is true of $\tau \langle \nu - \nu_0 \rangle_\infty$ for all N; the boundary for $\tau \langle \nu - \bar{\nu} \rangle_\infty$ falls half as fast.
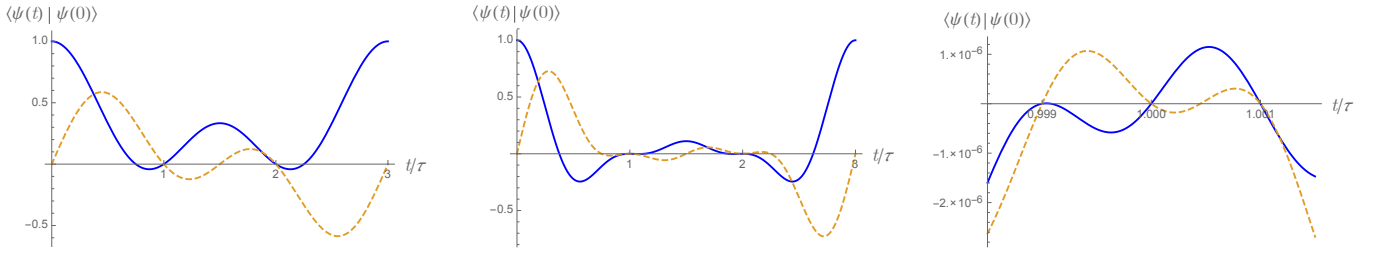
FIG. 9. **Almost-equal separations.** As in Figure 1, we show the real (solid) and imaginary (dashed) parts of the overlap function $\langle\psi(t)|\psi(0)\rangle$ of Equation (6), for $|\psi(t)\rangle$ that minimize $\langle\nu-\nu_0\rangle_1$ for a periodic evolution of length T with N distinct states. Left: All $N=3$ separations are of length $\tau=T/N$, and $\langle\nu-\nu_0\rangle_1 T=1$. Middle: Separations differ by one part in 10^3, and $\langle\nu-\nu_0\rangle_1 T\approx 2.001$. Right: Detail of flat region near $t/\tau=1$ from the middle graph. If we make the separations more equal, the oscillation gets narrower and its amplitude smaller. In the limit, only the extra constraint "slope $=0$ at $t/\tau=1$ and 2" keeps Middle distinct from Left, and $\langle\nu-\nu_0\rangle_1 T\to 2$.
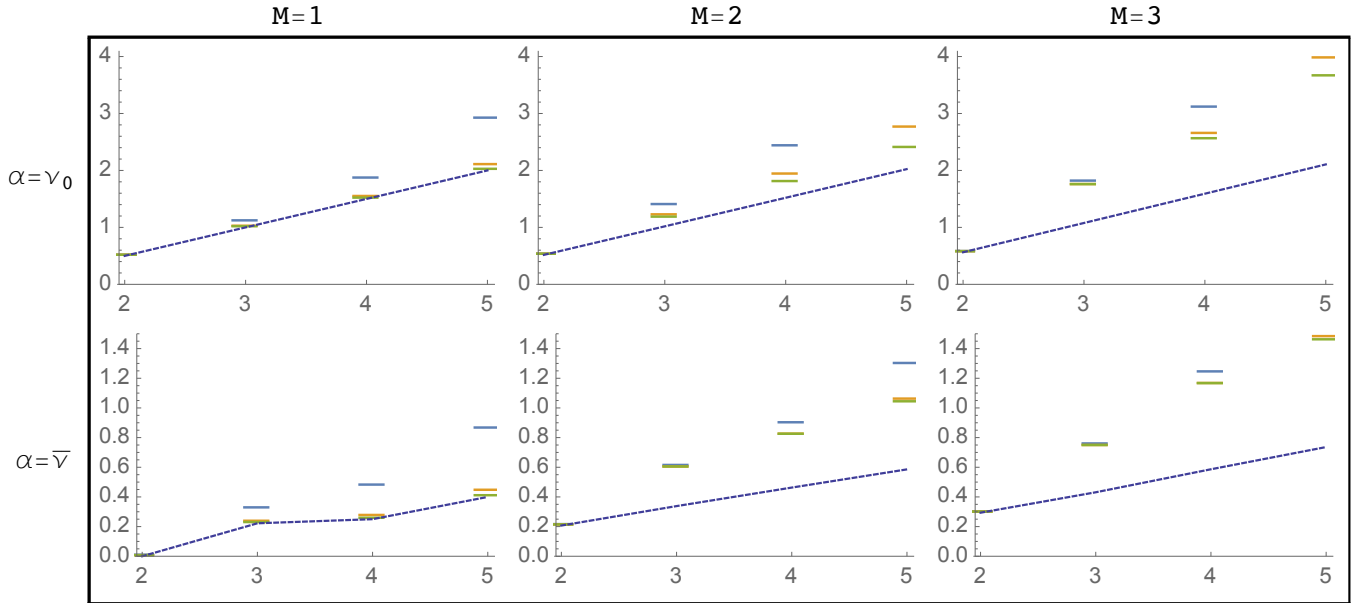

FIG. 10. **Extra width required by almost-equal separations, above that for equal ones.** All evolutions have period T. Vertical axes show the extra minimum-width of $\langle\nu-\alpha\rangle_M T$ for almost-equal separations, above the minimum needed for equal separations; horizontal axes show the number $N_{\text{different}}$ of different separations. The dashed lines are theoretical curves that minimize the width assuming we impose just the usual equal-separation constraints, along with slope $=0$ constraints at the equal separations. Triples of points correspond to separations that differ by one part in 10, 100 or 1000. The theoretical bounds shown seem tight for $M=1$ or for $N_{\text{different}}=2$.
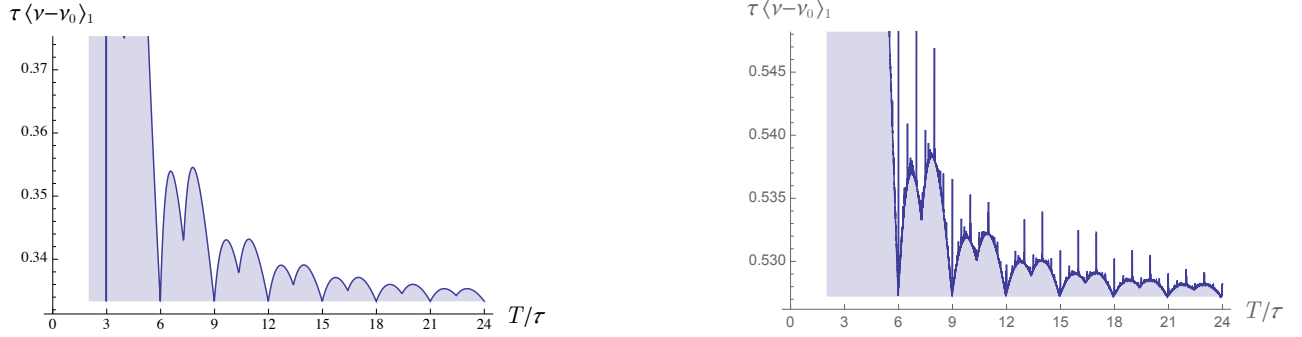
FIG. 11. Unequal separations in a portion of an evolution. Left: Minimum of $\tau \langle \nu - \nu_0 \rangle_1$ for two equal separations between three distinct states. Right: Two almost-equal separations require a larger $\tau \langle \nu - \nu_0 \rangle_1$. The unequal separations used here differ by one part in 10^3, and the spikes are not numerical artifacts. With equal separations the minimum is $1/3$; with the given unequal separations the minimum is about $.527$. The range shown on the right is only half that on the left.
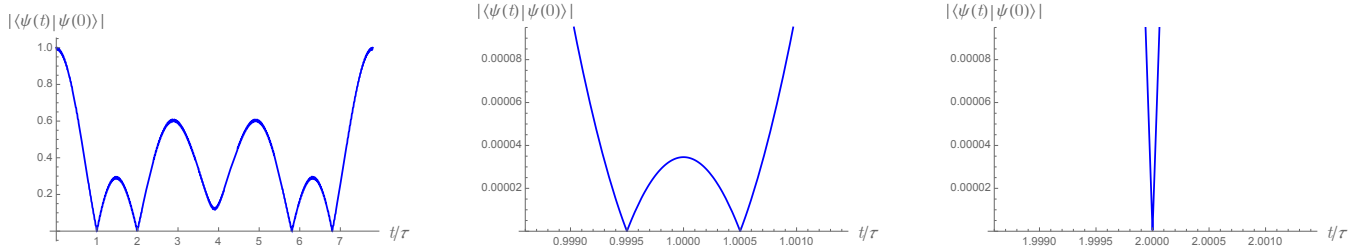

FIG. 12. Satisfying almost-equal orthogonality constraints. For the computation shown in Figure 11 (right), we look in detail at a particular value of the maximum period: for $T = 7.8\,\tau$ we plot the magnitude of the overlap function $\langle \psi(t)|\psi(0) \rangle$ of Equation (6) using the coefficients $|a_n|^2$ that minimize $\langle \nu - \nu_0 \rangle_1$. Left: Full-scale behavior. Middle: Detail near $t = \tau$. Right: Detail near $t = 2\tau$. The full scale graph depends strongly on our choice of T, but the detail graphs near τ and 2τ don't.
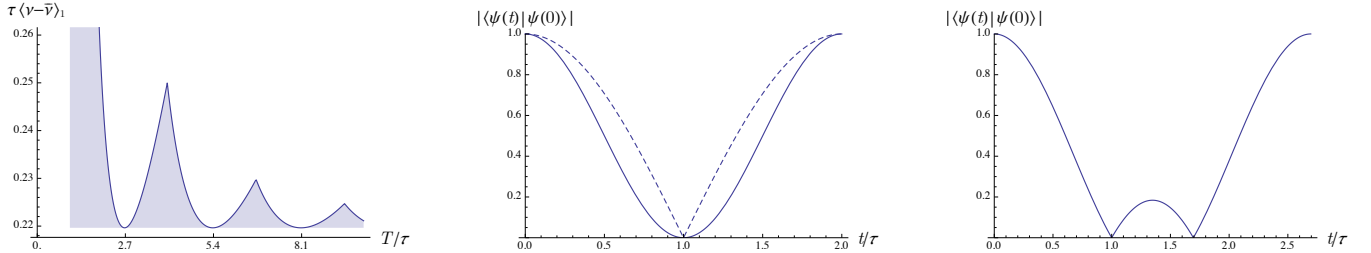

FIG. 13. First absolute moment about the mean with two distinct states. Left: If the two distinct states are separated by an interval τ, the global minimum of $\tau \langle \nu - \bar{\nu} \rangle_1$ is about $.22$, and repeats whenever the maximum period T of the evolution is an integer multiple of approximately 2.7τ. Middle: At $T = 2\tau$, a three-frequency-wide state (solid) achieves the same minimum $\tau \langle \nu - \bar{\nu} \rangle_1$ as a minimum-width two-frequency state (dashed). Right: The state that achieves the first global minimum at $T \approx 2.7\tau$ uses three frequencies. Knowing this, we can determine the minimum analytically by solving a transcendental equation: $f_{\bar{\nu}}(1, 2) \to u/2\pi$ where $u \approx 1.3801$ is a root of $u \sin(u + \sqrt{u^2 - 1}) = 1$.
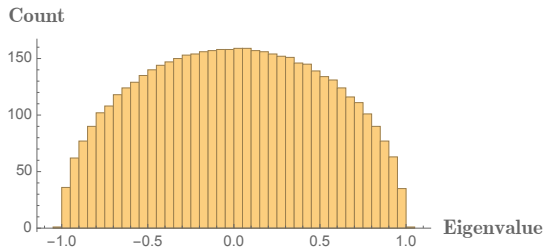
FIG. 14. *Distribution of eigenvalues for a* 5000×5000 *hermitian matrix with random entries.* The matrix has been normalized to give a fixed range of eigenvalues. Here the range is divided evenly into bins, and the number of eigenvalues in each bin is plotted. The shape is semicircular for almost any kind of randomness, if the width is plotted as twice the height.

Appendix B: Random hamiltonians

Wigner [66] observed that one can predict aspects of the behavior of complicated dynamics by studying the distribution of eigenvalues of hamiltonian matrices with random entries—a novel kind of statistical mechanics [67]. Here we review how eigenvalue statistics lead to a universal law governing how soon random hamiltonian evolution reaches a state orthogonal to a generic initial state [68].

The property of random hamiltonians that we use is illustrated in Figure 14. The histogram shows the number of eigenvalues that fall in equal-sized ranges for a 5000×5000 random hermitian matrix. The semicircular shape is universal, independent of the details of the randomness [69]. In the case shown, the hermitian matrix was constructed by adding a random complex matrix to its conjugate transpose, and then normalized by dividing by half-the-width of its eigenvalue range. The entries in the complex matrix had real and imaginary parts chosen uniformly between $-1/2$ and $+1/2$.

For an initial state $\psi(0) = \sum a_n |E_n\rangle$, the overlap with $\psi(t)$ depends only on the squared magnitudes $|a_n|^2$ and the energy eigenvalues E_n. If the initial state is randomly chosen, the eigenvalues in each range appear in the overlap about as frequently as they do in the semicircular distribution, so we can exactly compute the overlap in the infinite dimensional limit. For eigenvalues ranging from $-E$ to $+E$, letting $h = 2$, this has the universal form

$$\langle \psi(t) | \psi(0) \rangle = \int_{-1}^{1} e^{i\pi E u t} \frac{2}{\pi} \sqrt{1 - u^2} \, du$$

$$= \frac{2 J_1(\pi E t)}{\pi E t} , \qquad \text{(B1)}$$

where J_1 is a Bessel function. The factor $\sqrt{1 - u^2}$ is the height of a radius-one semicircle at position u. Multiplying this by $2/\pi$ gives the probability density for a semicircular distribution. If we take the lowest eigenvalue to be zero, E is the average energy.
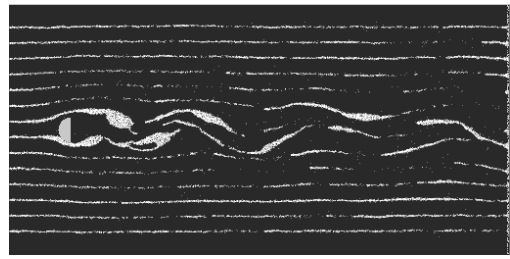

FIG. 15. *Realistic hydrodynamic flow in a finite-state lattice gas.* We first construct an idealized continuous dynamics where, if particles start at lattice locations with a discrete set of velocities, they are always found at lattice locations at integer times. We then simulate just the integer time behavior.
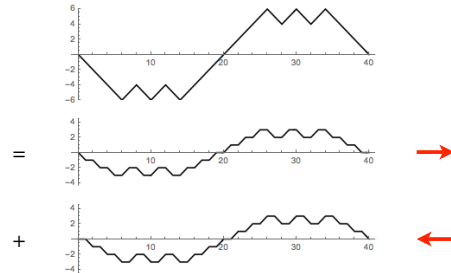

FIG. 16. *Continuous wave-equation in a finite-state lattice dynamics.* One dimensional wave behavior is a superposition of a right-going wave and a left-going wave. If the moving waves have discretely constrained shapes, then at integer times they exactly match the behavior of a simple local lattice dynamics.

Appendix C: Finite-state classical mechanics

Classical lattice gases, such as the Ising Model, have long played an important role in statistical mechanics [47]. Lattice gases have also been used to model dynamics. The simplest way to *exactly* map continuous quantities in classical mechanics onto a finite-state lattice is to first construct a continuous evolution that has discrete properties at integer times—and then just model the integer time behavior [27, 70–76] (*cf.* [53, 54]). For example, model a gas of idealized particles that, if started exactly in one of a finite number of configurations of positions and momenta, is always found in one of these configurations at integer times. As long as we only constrain the initial state to be discrete, and not the dynamical law itself, conservations still follow from continuous symmetries of the lagrangian.

Figure 15 illustrates a simple discrete-velocity lattice gas, constructed by restricting the initial positions and momenta of an idealized classical mechanical gas so that particles are always found on a triangular lattice at integer times. At large scales, and with relatively slow flow rates, the lattice-scale constraints on the initial state become invisible and the flow is hydrodynamic, with full rotational symmetry [71]. For visualization, a second lattice gas that follows the flow was added (shown in white). Similar models in three dimensions enable realistic hydrodynamic simulations of complex fluids [74].
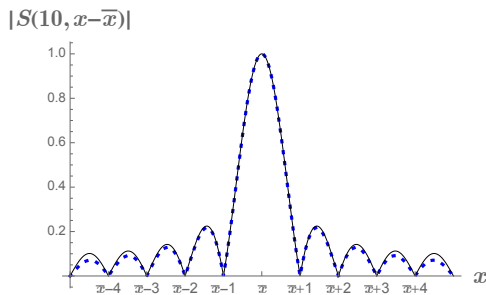
FIG. 17. *Magnitude of periodic sampling function.* One period of $|S(10, x - \bar{x})|$ is shown (solid), centered at position $\bar{x}$. Like the magnitude of the usual sinc sampling function (shown dotted), it is zero at integer separations from $\bar{x}$ (but is periodic).

Figure 16 provides a second example, illustrating how the continuous wave-equation can be simulated by simple finite-state lattice dynamics. Again we start with continuous motion—right and left going waves—and impose constraints on the initial state so that, at integer times, only configurations from a finite set are possible. The integer time behavior thus samples the continuous wave equation, albeit microscopically there are constraints on the detailed initial shape of the wave. This mechanism was actually discovered experimentally, in simple reversible cellular automata models of physics such as energy conserving Ising dynamics [75]. Exactly invertible lattice simulations of the wave equation can be implemented in any number of dimensions [77]. Similar examples [27] sample continuous relativistic dynamics.

Appendix D: Interpolated evolution

The quantum formalism provides a natural mechanism for turning a discrete evolution into a continuous one [26]. If, for example, we define a unitary U_τ that performs a discrete logic operation on qubits in a fixed time τ, we can find a hamiltonian H that generates U_τ in time τ:

$$\mathsf{U}_\tau = e^{-2\pi i \mathsf{H}\tau/h} . \tag{D1}$$

Any such H defines an evolution not only at intervals τ, but also for any other time interval t, with $\mathsf{U}_t = e^{-2\pi i \mathsf{H} t/h}$.

Constructing an H from a discrete evolution is a kind of interpolation [21] that turns a set of samples at discrete times into a continuous evolution. To illustrate the connection to classical interpolation, consider a simple classical finite-state evolution: at integer multiples of time τ, a single 1 appears at consecutive integer positions of a 1D periodic space of width N. All other integer positions contain 0's at these times. We construct an H that implements this discrete logical shift as part of a continuous-time quantum evolution that achieves the average energy bound (3) on distinct state change.

We take the N distinct logical configurations as basis states. Let $|n\rangle$ be the state where the 1 is at position n,

and $|n+1\rangle = \mathsf{U}_\tau |n\rangle$. Define another set of basis vectors $\{|k\rangle\}$ as the fourier transform of the position basis $\{|n\rangle\}$:

$$|k\rangle = \frac{1}{\sqrt{N}} \sum_{n=0}^{N-1} e^{+2\pi i n k / N} |n\rangle \tag{D2}$$

for integers $k \in [0, N-1]$. The inverse transform is then

$$|n\rangle = \frac{1}{\sqrt{N}} \sum_{k=0}^{N-1} e^{-2\pi i n k / N} |k\rangle . \tag{D3}$$

Define H by letting each $|k\rangle$ be an energy eigenstate, with energy eigenvalue $E_k = kh/N\tau$. Then if $\mathsf{U}_t = e^{-2\pi i \mathsf{H} t/h}$,

$$\mathsf{U}_\tau |n\rangle = \frac{1}{\sqrt{N}} \sum_{k=0}^{N-1} e^{-2\pi i (n+1)k/N} |k\rangle$$

$$= |n+1\rangle , \tag{D4}$$

which is the desired discrete evolution. We see from (D3) that $|n\rangle$ is an equally weighted superposition of equally separated energy eigenstates, so this evolution achieves the average energy bound on distinct state change.

Given H, the state at any continuous time t can be expressed in terms of the integer-position basis states. Starting with the particle in a basis state at position 0,

$$\mathsf{U}_t |0\rangle = \frac{1}{\sqrt{N}} \sum_{k=0}^{N-1} e^{-2\pi i k t / N\tau} |k\rangle$$

$$= \frac{1}{N} \sum_{k=0}^{N-1} e^{-2\pi i k t / N\tau} \sum_{n=0}^{N-1} e^{+2\pi i n k / N} |n\rangle$$

$$= \sum_{n=0}^{N-1} S(N, n - t/\tau) |n\rangle , \tag{D5}$$

where

$$S(N, u) = \frac{1}{N} \sum_{k=0}^{N-1} e^{2\pi i k u / N} \tag{D6}$$

is a periodic version of the sampling function $\operatorname{sinc} \pi u = \sin \pi u / \pi u$, which is the foundation of bandlimited interpolation theory. This is illustrated in Figure 17. In fact, $S(N, u) \to e^{i\pi u} \operatorname{sinc} \pi u$ for $N \to \infty$. For t/τ an integer, only one configuration $|n\rangle$ in (D5) has a non-zero coefficient. At all other times, $S(N, n - t/\tau)$ is not centered at an integer, and all $|n\rangle$ have non-zero coefficients.

Appendix E: Sampled evolution

A continuous evolution is equivalent to a discrete one if the continuous is just an interpolation of the discrete: then there is no more information in the continuous than in the discrete [21–35]. This equivalence is the basis of

sampling theory: a finite-bandwidth periodic signal has only a finite number of terms in its Fourier series, so once enough discrete samples of the signal have been taken to determine the coefficients of all terms, there is no more information in the signal. The signal is effectively discrete.

The same logic applies to quantum systems: if the evolution is periodic and uses only a finite range of energy frequencies, then knowing a finite number of samples $|\psi(t_k)\rangle$ of the continuous (vector) signal $|\psi(t)\rangle$ determines the rest. This implies that finite-sized quantum systems with finite energy are effectively discrete, since their evolution is arbitrarily close to one cycle of an exactly recurrent evolution with finite bandwidth [41].

As an illustration of sampling a quantum evolution [26], consider a scalar wavefunction $\psi(x,t)$ that has a periodic evolution with period T, and a range of energy eigenfrequencies of width $(K-1)/T$, with $E_0 = 0$. Using units of time where $T = K$, we see that the state at all times is just an interpolation of the state at integer times:

$$\psi(x,t) = \sum_{k=0}^{K-1} \psi(x,k)\, S(K, k-t)\,, \qquad \text{(E1)}$$

where S is the sampling function (D6). This identity is obvious if t is an integer between 0 and $K-1$, since then $S(K, k-t) = \delta_{k,t}$. Hence (E1) holds for all t, since both sides add together the same K Fourier components, and the K integer-t cases determine all coefficients in the sum.

This identity applies to the discrete shift example of Appendix D, recast as a continuous shift of a finite-bandwidth state: $\mathsf{H} = v\mathsf{p}_x$, with $v = 1$, and using only a finite range of momenta in a periodic space. To have N distinct states requires $K \geq N$, and to achieve the minimum bandwidth we must use an equal superposition of equally separated eigenstates, which is just $\psi(x,t) = S(N, x-t)$. This evolution is a continuous interpolation of a discrete (integer x and t) binary shift.

[1] M. Planck, *Ueber das gesetz der energieverteilung im normalspectrum*, Ann. Phys. (Berlin) **309**, 553 (1901).

[2] M. Planck, *Die physikalische struktur des phasenraumes*, Ann. Phys. (Berlin) **355**, 385 (1916).

[3] L. de Broglie, *Recherches sur la théorie des quanta*, Ann. de Physique **3**, 22 (1925).

[4] E. Schrödinger, *An undulatory theory of the mechanics of atoms and molecules*, Phys. Rev. **28**, 1049 (1926).

[5] N. Bohr, *The quantum postulate and the recent development of atomic theory*, Nature **121**, 580 (1928).

[6] W. Heisenberg, *Über den anschaulichen inhalt der quantentheoretischen kinematik und mechanik*, Z. Phys. **43**, 172 (1927).

[7] L. Mandelstam and I. Tamm, *The uncertainty relation between energy and time in non-relativistic quantum mechanics*, J. Phys. (USSR) **9**, 249 (1945).

[8] K. Bhattacharyya, *Quantum decay and the Mandelstam-Tamm-energy inequality*, J. Phys. A **16**, 2993 (1983).

[9] J. Uffink and J. Hilgevoord, *Uncertainty principle and uncertainty relations*, Found. Phys. **15**, 925 (1985).

[10] D. Donoho and P. Stark, *Uncertainty principles and signal recovery*, SIAM J. Appl. Math. **49**, 906 (1989).

[11] S. Braunstein, C. Caves and G. Milburn, *Generalized uncertainty relations*, Ann. Phys. **247**, 135 (1996).

[12] T. Yu, *A note on the uncertainty relation between the position and momentum*, Phys. Lett. A **223**, 9 (1996).

[13] N. Margolus and L. B. Levitin, *The maximum speed of dynamical evolution*, Physica D **120**, 188 (1998).

[14] V. Giovannetti, S. Lloyd and L. Maccone, *Quantum limits to dynamical evolution*, Phys. Rev. A **67**, 052109 (2003).

[15] S. Luo and Z. Zhang, *On decaying rate of quantum states*, Lett. Math. Phys. **71**, 1 (2005).

[16] B. Zieliński and M. Zych, *Generalization of the Margolus-Levitin bound*, Phys. Rev. A **74**, 034301 (2006).

[17] H. F. Chau, *Tight upper bound of the maximum speed of evolution of a quantum state*, Phys. Rev. A **81**, 062133 (2010).

[18] S. Zozor, M. Portesi, P. Sanchez-Moreno and J. S. Dehesa, *Position-momentum uncertainty relations based on moments of arbitrary order*, Phys. Rev. A **83**, 052107 (2011).

[19] J. C. Angulo, *Generalized position-momentum uncertainty products*, Phys. Rev. A **83**, 062102 (2011).

[20] H. Nyquist, *Certain topics in telegraph transmission theory*, Trans. Am. Inst. Elec. Eng. **47**, 617 (1928).

[21] E. Meijering, *A chronology of interpolation*, Proc. IEEE **90**, 319 (2002).

[22] A. Kempf, *Fields over unsharp coordinates*, Phys. Rev. Lett. **85**, 2873 (2000).

[23] A. Kempf, *Spacetime could be simultaneously continuous and discrete, in the same way that information can be*, New J. Phys. **12**, 115001 (2010).

[24] S. Hossenfelder, *Minimal length scale scenarios for quantum gravity*, Living Rev. Relativity, **16**, 2 (2013).

[25] M. Tsang, J. Shapiro and S. Lloyd, *Quantum theory of optical temporal phase and instantaneous frequency*, Phys. Rev. A **78**, 053820 (2008).

[26] N. Margolus, *Quantum emulation of classical dynamics*, arXiv:1109.4995v3 (2011).

[27] N. Margolus, *The ideal energy of classical lattice dynamics*, Lect. Notes Comput. Sc. **9099**, 169 (2015).

[28] S. Succi and R. Benzi, *Lattice Boltzmann equation for quantum mechanics*, Physica D **69**, 327 (1993).

[29] I. Bialynicki-Birula, *Weyl, Dirac, and Maxwell equations on a lattice as unitary cellular automata*, Phys. Rev. D **49**, 6920 (1994).

[30] D. A. Meyer, *From quantum cellular automata to quantum lattice gases*, J. Stat. Phys. **85**, 551 (1996).

[31] J. Yepez, *Relativistic path integral as a lattice-based quantum algorithm*, Quantum Inf. Process. **4**, 471 (2005).

[32] J. Yepez, *Quantum informational model of 3+1 dimensional gravitational dynamics*, Proc. SPIE **7702**, 770202 (2010).

[33] J. Yepez, *Quantum lattice gas algorithmic representation of gauge field theory*, Proc. SPIE **9996**, 99960N (2016).

[34] M. Dalmonte and S. Montangero, *Lattice gauge theories simulations in the quantum information era*, Contemp. Phys. **57**, 388 (2016).

[35] G. M. D'Ariano, *Physics without physics: the power of information-theoretical principles*, Int. J. Theor. Phys. **56**,

97 (2017).

[36] P. Kok, S. Braunstein and J. Dowling, *Quantum lithography, entanglement and Heisenberg-limited parameter estimation*, J. Opt. B **6**, S811 (2004).

[37] V. Giovannetti, S. Lloyd and L. Maccone, *Quantum-enhanced measurements*, Science **306**, 1330 (2004).

[38] V. Giovannetti, S. Lloyd and L. Maccone, *Quantum measurement bounds beyond the uncertainty relations*, Phys. Rev. Lett. **108**, 260405 (2012).

[39] M. J. W. Hall, D. W. Berry, M. Zwierz and H. W. Wiseman, *Universality of the Heisenberg limit for estimates of random phase shifts*, Phys. Rev. A **85**, 041802 (2012).

[40] M. Zwierz, C. A. Pérez-Delgado and P. Kok, *Ultimate limits to quantum metrology and the meaning of the Heisenberg limit*, Phys. Rev. A **85**, 042112 (2012).

[41] P. Bocchieri and A. Loinger, *Quantum recurrence theorem*, Phys. Rev. **107**, 337 (1957).

[42] R. Verch, *On generalizations of the spectrum condition*, Fields Inst. Commun. **30**, 409 (2001).

[43] G. Volovik, *Vacuum energy*, Int. J. Mod. Phys. D **15**, 1987 (2006).

[44] S. Luo, *Variation of the Heisenberg uncertainty relation involving an average*, J. Phys. A **34**, 3289 (2001).

[45] S. P. Jordan, *Fast quantum computation at arbitrarily low energy*, Phys. Rev. A **95**, 032305 (2017).

[46] S. Morley-Short, L. Rosenfeld and P. Kok, *Unitary evolution and the distinguishability of quantum states*, Phys. Rev. A **90**, 062116 (2014).

[47] D. Ruelle, *Statistical Mechanics*, World Scientific (1999).

[48] T. Toffoli, *Cellular automata as an alternative to (rather than an approximation of) differential equations in modeling physics*, Physica D **10**, 117 (1984).

[49] E. Fredkin, *Digital mechanics*, Physica D **45**, 254 (1990).

[50] A. R. Brown, D. A. Roberts, L. Susskind, B. Swingle and Y. Zhao, *Holographic complexity equals bulk action?*, Phys. Rev. Lett. **116**, 191301 (2016).

[51] C. H. Bennett and D. P. DiVincenzo, *Quantum information and computation*, Nature **404**, 247 (2000).

[52] S. Lloyd, *The quantum geometric limit*, arXiv:1206.6559v4 (2012).

[53] J. E. Marsden and M. West, *Discrete mechanics and variational integrators*, Acta Numerica **10**, 357 (2001).

[54] B. Bahr and B. Dittrich, *Improved and perfect actions in discrete gravity*, Phys. Rev. D **80**, 124030 (2009).

[55] S. W. Hawking, *Breakdown of predictability in gravitational collapse*, Phys. Rev. D **14**, 2460 (1976).

[56] S. Braunstein, S. Pirandola and K. Życzkowski, *Better Late than Never: Information Retrieval from Black Holes*, Phys. Rev. Lett. **110**, 101301 (2013).

[57] W. G. Unruh and R. M. Wald, *Information loss*, arXiv:1703.02140v1 (2017).

[58] J. D. Bekenstein, *Black holes and entropy*, Phys. Rev. D **7**, 2333 (1973).

[59] T. Jacobson, *Thermodynamics of spacetime: the Einstein equation of state*, Phys. Rev. Lett. **75**, 1260 (1995).

[60] T. Padmanabhan, *Thermodynamical aspects of gravity: new insights*, Rep. Prog. Phys. **73**, 046901 (2010).

[61] E. Verlinde, *On the origin of gravity and the laws of Newton*, J. High Energ. Phys. 04 (2011) 029.

[62] W. G. Unruh, *Sonic analogue of black holes and the effects of high frequencies on black hole evaporation*, Phys. Rev. D **51**, 2827 (1995).

[63] G. 't Hooft, *Quantum gravity as a dissipative deterministic system*, Class. Quantum Grav. **16**, 3263 (1999).

[64] P. O. Mazur and E. Mottola, *Gravitational vacuum condensate stars*, Proc. Natl. Acad. Sci. U.S.A. **101**, 9545 (2004).

[65] N. Margolus, *Mathematica numerical tests for the paper, "The finite state character of physical dynamics"*. Download http://arxiv.org/src/1109.4994 and open the file anc/numerical-tests.nb

[66] E. P. Wigner, *Characteristic vectors of bordered matrices with infinite dimensions*, Ann. Math. **62**, 548 (1955).

[67] T. Guhr, A. Müller-Groeling and H. A. Weidenmüller, *Random-matrix theories in quantum physics: common concepts*, Physics Reports **299**, 189 (1998).

[68] E. J. Torres-Herrera, J. Karp, M. Távora and L. F. Santos, *Realistic many-body quantum systems vs full random matrices: static and dynamical properties*, Entropy **18**, 359 (2016).

[69] L. Erdős, *Universality of Wigner random matrices: a survey of recent results*, Russian Math. Surveys **66**, 507 (2011).

[70] E. Fredkin and T. Toffoli, *Conservative logic*, Int. J. Theor. Phys. **21**, 219 (1982).

[71] U. Frisch, B. Hasslacher and Y. Pomeau, *Lattice-gas automata for the Navier-Stokes equation*, Phys. Rev. Lett. **56**, 1505 (1986).

[72] N. Margolus, T. Toffoli and G. Vichniac, *Cellular-automata supercomputers for fluid dynamics modeling*, Phys. Rev. Lett. **56**, 1694 (1986).

[73] J. Salem and S. Wolfram, *Thermodynamics and hydrodynamics of cellular automata*, in Theory and applications of cellular automata (Wolfram, ed.), World Scientific, 362 (1986).

[74] D. Rothman and S. Zaleski, *Lattice-Gas Cellular Automata: Simple Models of Complex Hydrodynamics*, Cambridge University Press (1997).

[75] N. Margolus, *Crystalline computation*, in Feynman and Computation (Hey, ed.), Perseus Books Reading MA, 267 (1998).

[76] N. Margolus, *Universal cellular automata based on the collisions of soft spheres*, in New Constructions in Cellular Automata (Griffeath and Moore eds.), Oxford University Press, 231 (2003).

[77] H. J. Hrgovčić, *Discrete representations of the n-dimensional wave-equation*, J. Phys. A **25**, 1329 (1992).